Trans. JWRI, Vol. 25(1996), No.2

Modeling Activities in Japan

by Nobutaka Yurioka and Toshihiko Koseki

Abstract

The history of modeling weld phenomena in Japan can be traced back to 1940's. One early study worthy of note is the Tanaka solution to welding heat conduction, which was published in 1943, two years after Rosenthal's solution. Since then, a number of modeling activities have been carried out on various welding phenomena. In relation to the welding of C-Mn and low alloy steels, primary efforts have concentrated on improving the prediction of HAZ hardness and cold cracking susceptibility of weldments. In this respect, the present paper reviews the analytical and experimental modeling of heat conduction, hardenability, hydrogen diffusion, and residual stress carried out in Japan. The modeling of weld pool behavior, solidification and phase transformation has also been attempted to predict weld microstructure and weldability. In some recent studies, a thermodynamic calculation method has been introduced to improve the modeling of multicomponent steels.

1. Introduction

The original of this review paper was presented in "Third International Seminar on Numerical Analysis of Weldability" which was held in Graz, Austria in 1995 under the organization by Professors H. Cerjak and H. K. D. H. Bhadeshia. Three consecutive seminars on this issue ended in success, suggesting that the modeling activities in welding have been increasingly intensive worldwide. The authors felt that Japanese activities on the modeling of welding phenomena are relatively unknown in the world because they are reported mostly in Japanese. Then the authors have revised some parts in the original paper, emphasizing the originality of Japanese work.

The modeling of weld phenomena in Japan, as well as in Europe and the USA, started in early 1940's. One noteworthy result of the early studies is the Tanaka analytical solution[1] to welding heat conduction in 1943, just two years after Rosenthal's solution[2] Since Tanaka considered surface heat transfer assuming a surface heat source, his solution is more general than Rosenthal's. Another important aspect of the early work in Japan was the elastic analysis of welding transient stresses started in early 1950's. Masubuchi[3] introduced the concept of "inherent residual strain" to facilitate the analysis of welding residual stresses and distortion without conducting the step-by-step calculation of transient strain during post-solidification cooling.

The term of "weldability" emerged in Japan in the mid 1950's when sulfur cracks were found in steel plates when the plates were welded in shipyards. Since then, efforts toward the improvement of steel weldability have continued primarily by steel manufacturers. The trend of modeling activities has reflected the progress of steels and changes in the users' requirements of weldability. In 1968, Itoh et al.[4] proposed Pcm carbon equivalent to assess weldability or cold cracking susceptibility of steels, while the carbon equivalent for steel weldability was first proposed by Dearden and O'Neil[5] in 1940. Since then, many researches have been conducted on weldability and hardenability of carbon-manganese and low alloy steels. The modeling of the welding of stainless steels is a relatively new area, and has been necessitated by the in-

Transactions of JWRI is published by Joining and Welding Research Institute of Osaka University, Ibaraki, Osaka567, Japan.

creasing applications of stainless steels in various hostile environments in chemical and power plants.

Mathematical modeling of weld phenomena have been increasingly active in Japan together with the development of computer-assisted numerical analysis and metallurgical phase calculation based on thermodynamic data, as so in Europe and U.S. This paper reviews the Japanese activities on heat conduction, weld, solidification, phase trans-formation, harden-ability, hydrogen diffusion, residual stress, weld distortion and cold cracking.

2. Heat Conduction

The weld thermal history is one of the major factors which determines cracking susceptibility and weldment performances as well as residual stresses and strains within a welded structure. The microstructure and hardness of the HAZ, for example, are often estimated from the cooling time from 800℃ to 500℃ ($t_{8/5}$), and the HAZ cold cracking susceptibility from the cooling time down to 100℃ (t_{100})[6] ; $t_{8/5}$ more or less governs austenite(γ)-to-ferrite(α) transformation, and t_{100} represents the time over which hydrogen diffusion can take place in welds. Terasaki et al.[7] developed a simpler model for the prediction of $t_{8/5}$. Yurioka et al.[8] showed that, when preheating is employed, $t_{8/5}$ can be estimated by linearly combining the heat conduction of welding with that of uniform preheating. However, this is not the case for t_{100} which can vary with the size of panel and the method of preheating. The Tanaka solution may no longer be applicable when a welded plate size is smaller than the diffusion distance of heat in the period of t_{100}. Initial temperature profiles produced by preheating also exert a large influence on t_{100}, and the assumption of uniform preheating may be invalid.

When the weld penetration is comparable to the plate thickness in high heat-input welding, existing models for weld heat conduction are unable to provide a re-presentative shape of either the weld pool or HAZ. In addition, they do not accurately predict the thermal history of different points within the HAZ. To

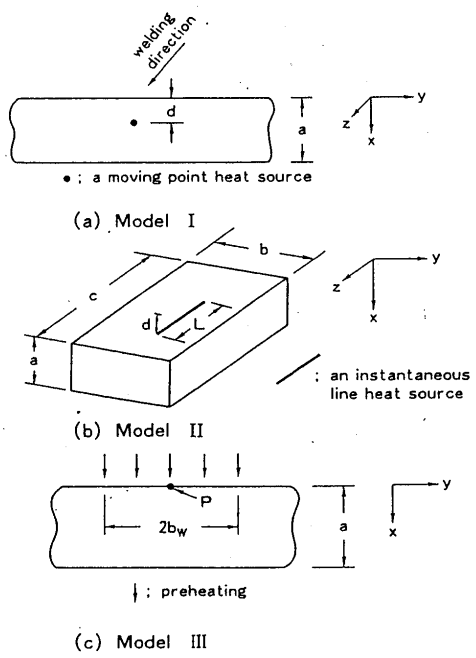

Fig. 1 Schematics of the models for weld heat conduction [10]

achieve good HAZ fracture toughness in C-Mn and low alloy steels for low temperature service, the size of intercritically reheated regions should be minimized[9] In this case, any heat conduction analysis using the surface point heat source assumption is inappropriate for the prediction of the thermal history of any specific point of the HAZ, and for the prediction of the size and location of these brittle region. In other words, the application of the Rosenthal and Tanaka solutions is limited to cases where high accuracy is not essential and is unsuitable for the prediction of weldment thermal history.

Kasuya and Yurioka[10] recently modeled three important heat conduction situations of welding, as shown in **Figure 1**, to overcome the above problems. Model I is based on a quasi-steady-state situation with a moving point heat source located within a plate of a finite thickness without neglecting surface heat transfer. Starting from a three dimensional, non-steady state general solution, they obtained the following analytical solution to the quasi-steady-state situation case:

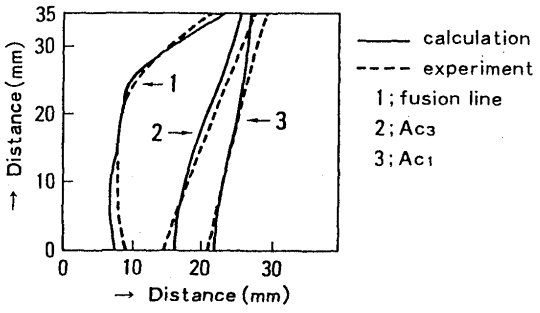

Fig. 2 Simulation of isotherms at HAZ of large heat-inpuct SA welding [10]

$$\theta = \frac{q}{\pi a \lambda} \sum_{n=1}^{\infty} A_n \left\{ \cos\left(\frac{u_n}{a} x\right) + \frac{Bi}{u_n} \sin\left(\frac{u_n}{a} x\right) \right\} \exp\left\{ -\frac{v_s (z - v_s t)}{2\kappa} \right\} K_0 \left\{ r \sqrt{\frac{u_n^2}{a^2} + \frac{v_s^2}{4\kappa^2}} \right\} \quad (1)$$

In the equation, θ is the temperature relative to the ambient temperature, q is the welding heat input, a is the plate thickness, λ is the thermal conductivity, u_n is the n-th eigenvalue, B_i is the Biot number ($=a\,\alpha / \lambda$), α is the surface heat transfer coefficient, k is the thermal diffusivity, and v_S is the welding, velocity along the z-axis. A_n and r are given by

$$\frac{u_n^2}{u_n^2 + B_i^2 + 2B_i} \left\{ \cos\left(\frac{u_n}{a} d\right) + \frac{B_i}{u_n} \sin\left(\frac{u_n}{a} d\right) \right\} \quad \text{and} \quad \sqrt{y^2 + (z - v_s t)^2}$$

, respectively, where d is the depth of the heat source from the plate surface. Obviously, Equation (1) can be reduced to the Tanaka solution by letting d be zero. The advantage of this solution is that a heat source can be located arbitrarily inside a plate, and therefore, any shape of weld pool with different heat inputs can be modeled by distributing multiple heat sources within a plate properly. Modeling was made for a single-pass submerged arc (SA) weld with triple electrodes (welding heat input :25kJ/mm) under low α covered flux insulation. The prediction is in a good agreement with experiment in terms of the shape of the fusion line and of HAZ isotherms; comparisons of the fusion line and isotherms for Ac_3 and Ac_1 are shown in **Figure 2**.

The other two heat conduction models are based on the instantaneous line heating of a plate of finite dimensions (Model II) and on the local preheating of a plate (Model 111)[10]. Schematics for these two models are shown in Figure 1. Analytical solutions to both situations were obtained using the same approach as employed in the above quasi-steady-state prob-lem but with modified initial conditions. The Model II is for a cold cracking test using a small test piece. The t_{100} of a small welded test piece differs from that of an actual welded plate due to a limited length available for thermal diffusion in the former. Thus, the model is useful in compensating for this difference and allowing the test result to be put to practical use. The Model III is for a local preheating with different heating powers. This problem is based on a fact that tem-perature profile within a plate prior to welding varies with preheating power input, and this significantly affects the subsequent thermal cycle of welding. **Figure 3** shows calculated temperature profiles within a 30mm-thick plate after preheating the plate surface (point P) up to 200℃ with two different power inputs but the same heating width. The internal temperature gradient is basically in the horizontal direction at the lower power input, while it is more vertical at the higher power input. Starting from these two initial profiles and using the linear combination of Models I and III, calculation of t_{100} indicates that preheating with the lower power input results in longer t_{100}; this corresponds well with practical experiences as described later in the section of cold cracking"

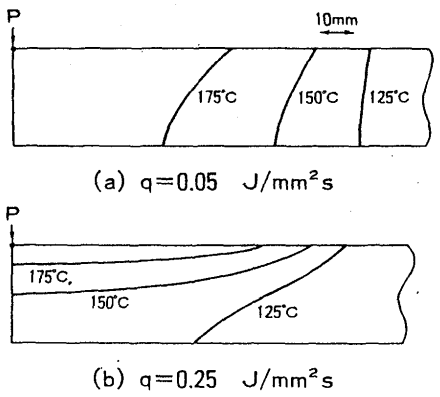

Fig. 3 Temperature distribution of a plate preheated with different preheating power [10]

Regarding a numerical approach to the quasi-steady state heat conduction on welding, Ushio and Ishimura[11] presented an algorithm for the time-independent Stefan problem to

predict more accurately the shape of a weld pool and isotherms in its vicinity. This problem deals with a free boundary between a liquid weld pool and a solid base metal, considering latent heat of fusion, heat conductivity and specific heat in liquid an solid. **Figure 4** compares their numerical analysis with the Rosenthal solution in terms of isotherms on a plate surface. It is apparent It is the isotherms are more contracted in the front and expanded to the back of the pool in the numerical analysis attributed to the fact that the latent heat of fusion, L^* and the thermal conductivity ratio between solid and liquid, λ^* have been taken into account.

Nakatani and Ohji[12] worked on an algorithm for inverse heat conduction problems in welding , by which the shape of a weld pool can be estimated from measured temperature profiles in the vicinity of the pool. They applied techniques of linear programming to the optimization of temperature fields. The objective function, F, is :

$$F = \sum_{i=1}^{N} \left(T_i^0 - T_i(q_1, q_2, \cdots, q_n) \right)^2 \qquad (2)$$

where T_i^0 is temperature measured at the point Pi and $Ti(q_1, q_2, .. q_n)$ is the theoretical temperature for the same point as shown in **Figure 5**. Theoretical temperatures are given by an analytical solution, e.g., the Rosenthal solution in their case, with a set of point heat sources. Through the optimization of a finite set of temperature measurements, the distribution of point heat sources, $(q_1, q_2, .. q_n)$ is finally determined. In Kasuyas' solution (Figure 2) , point heat sources were arbitrarily distributed but their solution should be improved if this inverse problem is applied to determine the distribution of heat sources rationally.

3. Weld Pool Behavior

The modeling of weld pool behavior has been performed for various purposes. The modeling of fluid flow in a weld pool has attracted particular attention in recent years, as the effects of chemistry on weld penetration were highlighted by experiment[13-15]. Surface active elements such as sulfur and oxygen were found to increase the depth of penetration. This

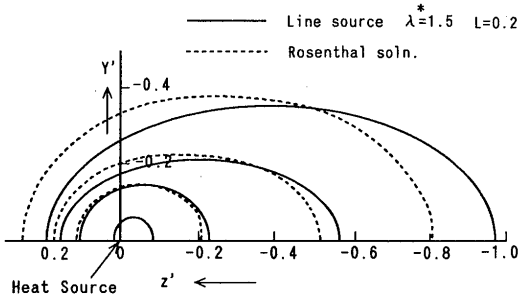

Fig. 4 Fusion lines produced by a line heat source with different heat inputs by numerical modeling [11]

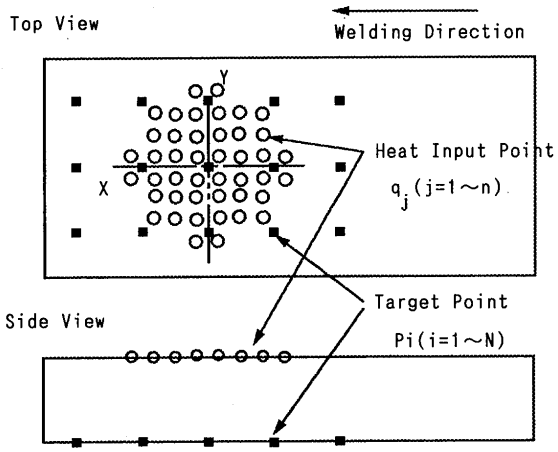

Fig. 5 Allocation of point heat sources and target measuring points [12]

effect was explained in terms of surface tension driven flow (i.e., Marangoni convection) in a weld pool since these elements modify the surface tension of the melt significantly[13-15]. To verify this assumption, the Marangoni convection was taken into account in the numerical modeling of weld pool behavior. Many models have demonstrated that the Marangoni convection dominates the shape of weld penetration[16, 17], and it seems thus far that the assumption on the chemistry effects is convincing.

Yokoya et al.[18] recently modeled non-steady state heat and mass transfer in a stationary GTA (Gas Tungsten Arc) weld pool considering fourfactors:i.e., electro-magnetic force, buoyancy, surface tension, and the aerodynamic drag force of arc plasma as shown in **Figure 6**. It was revealed that the surface tension driven flow affects the penetration only in a short arc process but the effect becomes insignificant as arc length increases and in this

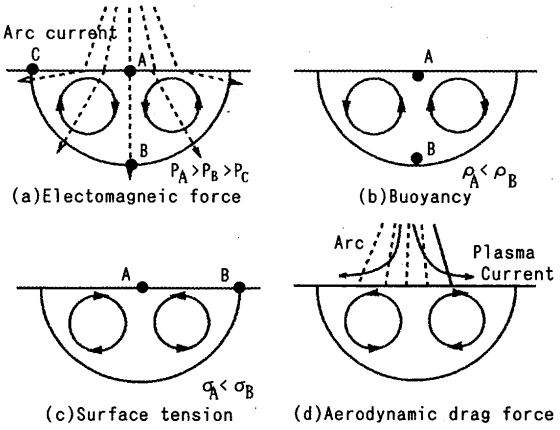

Fig. 6 Fluid flow in weld pool driven by four different forces [18]

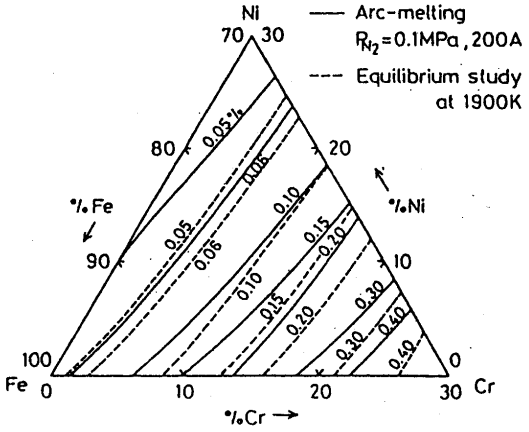

Fig. 7 Nitrogen solubility by experiment and equilibrium calculation [19]

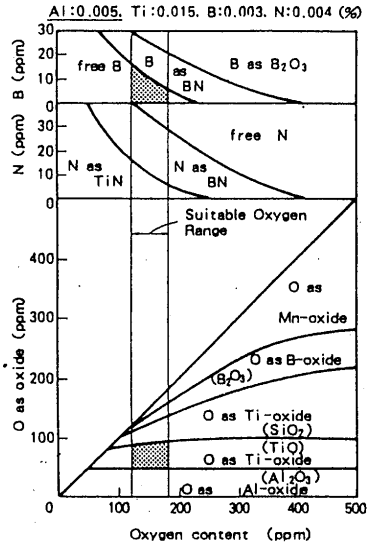

Fig. 8 Effect of oxygen on oxide composition and state of B and N [22]

instance the aerodynamic drag effect becomes dominant.

Gas absorption by a weld pool is another subject of interest in the modeling of weld pool behavior. Kuwana et al.[19] investigated the nitrogen absorption of Fe-Cr-Ni alloy weld metal during GTA welding with 1-atm. N_2 shielding gas. They compared the experimental results with thermodynamic prediction, and found that, even under the welding arc, the nitrogen solubility of the melt does not differ from the equilibrium solubility calculated for Fe-Cr-Ni melts as shown in **Figure 7**. Studies were extended to oxygen absorption by Sato et al.[20] and the solubility of a weld pool was again compared with theoretical prediction.

Chemical reactions within the weld pool are also an important issue to be considered in weld pool modeling. In low alloy steel weld metals, specific types of oxides act as nucleation sites for fine acicular ferrite within austenite grains, leading to significantly improved weld metal toughness[21]. This fact has been confirmed by a number of experiments, but the precise nature of the effective oxides and the mechanism of the nucleation of the acicular ferrite still remain poorly understood. Theoretical prediction of the formation of oxide inclusions in the melt would be helpful in addressing these issues. Horii et al.[21] estimated the fraction of each oxide formed in a SA weld pool, assuming that simple stoichiometric oxides were formed in the order of thermodynamic stability, and that the fraction was proportional to the relative amount of each oxidizer present in actual oxides extracted. **Figure 8** is an example of the results, where the fraction of nitrides was similarly estimated. They presumed based on their experimental observation that titanium oxides were needed for the nucleation of acicular ferrite as well as the presence of soluble boron. The calculation indicates the optimum range of oxygen content depending on aluminum content to obtain proper amount of titanium oxides. Some experimental results[22,23] indicate that 0.6 or thereabouts of [Al]/[O] ratio facilitates most effectively nucleation of intragranular ferrite.

Recently, the use of a CALPHAD software makes it possible to evaluate the phase

equilibria of multicomponent alloys, and thereby the formation of oxides in steel melts, including various complex oxides, can be analyzed from the equilibrium standpoint. **Figure 9** is an example of phase equilibria for the Fe base-Si-Mn-Ti-A1-N-O system at 1800 K, immediately above the solidification temperature, calculated by the authors [24] using Thermo Calc[25]. The system is widely used for low alloy weld metals, and in the calculation, nineteen oxides and two nitrides are considered as well as the liquid, δ-ferrite, austenite and slag. The formation of different oxides in the melt becomes feasible as the aluminum and titanium contents change. **Figure 10** is obtained from the isothermal phase diagram of Figure 9 by fixing titanium content at 0.01 wt%, showing the fraction of phases precipitated from the liquid phase against the [AI]/[0] ratio. This result implies that an aluminum-silicate (mullite) and a titanium oxide are formed preferentially in a SA weld metal with the [AI]/[0] ratio between 0.4 and 1.0. Furthermore, the calculation suggests that the mullite could undergo a transformation in austenite to galaxite ($MnO\,A1_2O_3$) which is considered to be an effective nucleant of accicular ferrite. However, this Thermo-Calc calculation on precipitation and transformation of oxides implies no role of titanium for accicular ferrite nucleation. The authors consider that titanium oxides, which is stable in the liquid phase, may act as nucleation sites for mullite and/or titanium of solid solution may accelerate transformation of mullite to galaxite in the solid phase.

Oxide formation in the interdendritic melt during solidification has been analyzed in steelmaking research by combining a solidification model with a CALPHAD method, and the model can be applied to welding without any significant modification. **Figure 11** [26] depicts the result of a calculation of oxide precipitation in the interdendritic melt during the solidification of a 18Cr-10Ni stainless steel with 0.5%Si-0.002%AI-0.0005%Ca-0.0004 % Mg 0.0004% O. In this calculation, dendritic solidification was analyzed by the Clyne-Kurz model[27], and oxide formation in the interdendritic melt was modeled using Thermo Calc[25]. It is indicated that the formation of SiO_2 increases in the interdendritic region as the

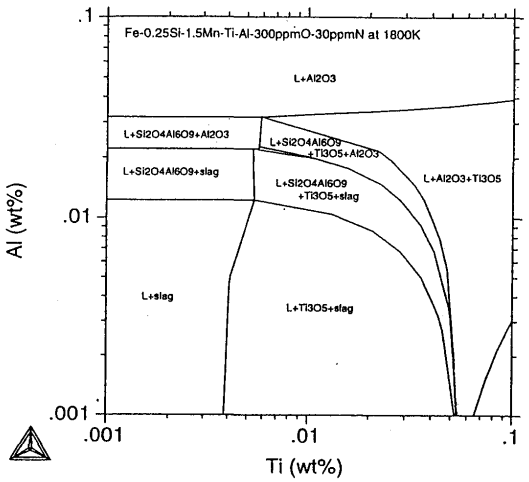

Fig. 9 Thermo–calc calculation for the formation of oxides in a SA weld pool at 1800K [24]

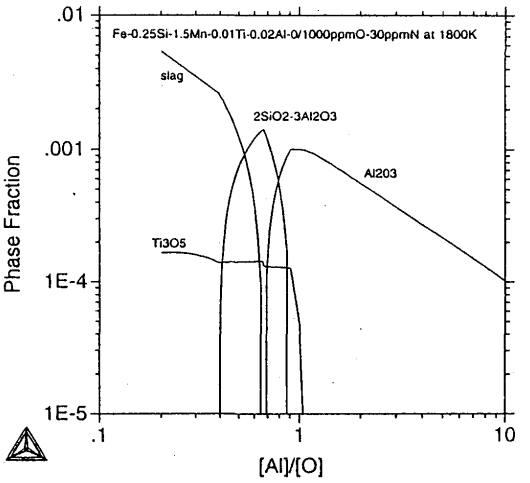

Fig. 10 Effect of Al/O ratio on fraction of phases precipitated from the liquid phase [24]

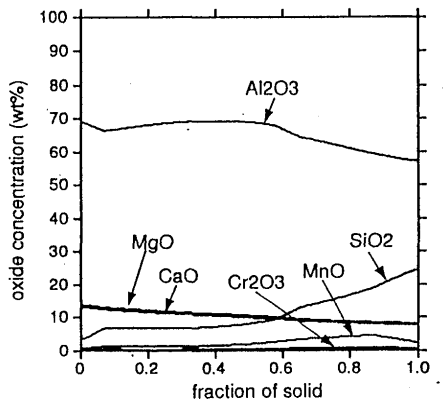

Fig. 11 Calculated compositions of non–metallic inclusions in the liquid during solidification [26]

interdendritic melt is enriched in Si with dendrite thickening, while the distribution oxides of stronger oxidizers such as Al, Ca and Mg is virtually uniform throughout the dendrite. Such results would be useful in controlling the type and distribution of oxides in weld metals especially when oxide dispersion is used to determine the phase transformation and subsequent performance of weld metals.

4. Solidification

Solute redistribution and phase chemistry during solidification are critical factors affecting subsequent phase trans-formation and final weld metal microstructure as well as hot cracking susceptibility on welding. As the melt solidifies, solute redistribution and resultant microsegregation are often estimated by simple analytical models which were originally developed for binary alloys, such as the Scheil model[28], the Brody-Flemings model[29] and the Clyne-Kurz model[27]. Those models are based on single phase solidification, and solute elements are treated independently without consideration of any interaction effects. However, this is not the case for multicomponent alloys; the partition ratio of each solute at the liquid/solid interface varies as solidification progresses, and multi-phase solidification through the peritectic or eutectic reaction is common.

Koseki et al. [30] developed a numerical model of the solidification and subsequent transformation of multicomponent alloy welds. A single cell with a hexagonal cross-section was assumed to grow into the melt, as illustrated in **Figure 12**, where heat conduction and solute diffusion were assumed to be longitudinal (i.e., along the cell axis) and radial, respectively. Calculation of kinetics was performed with a finite difference method (FDM) and combined with thermodynamic calculation using Thermo Calc[25]; solute partitioning, phase stability, and any other thermodynamic information in the alloy of interest were updated at each time-step for the FDM calculation. The advance of solidification, i.e., dendrite thickening, was evaluated by the heat balance between external heat extraction and latent heat evolution and also by local equilibrium at the solid/liquid interface. For the δ-to-γ solid state trans-

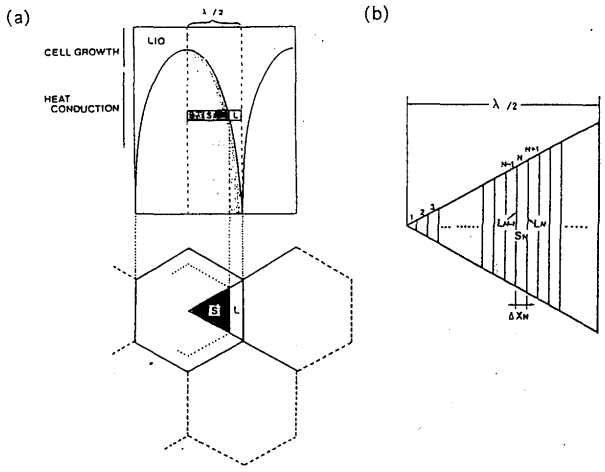

Fig. 12 (a) Longitudinal and transverse cross-sections of a solidifying cell, (b) segments for FDM analysis in transverse cross-section of the cell [30]

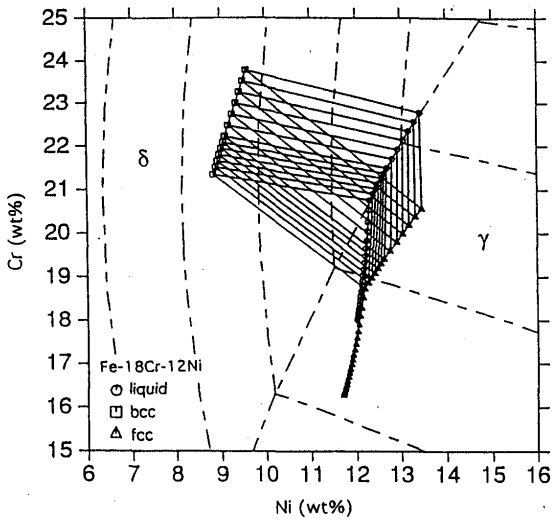

Fig. 13 Calculated solidification path of Fe–18Cr–12Ni stainless steel projected onto the liquidus surface [30]

formation in a FDM segment containing δ-ferrite, local equilibrium was assumed at the interface, and the extent of the transformation was determined by applying the Clyne-Kurz type analysis to each FDM segment.

The model was applied to the Fe-Cr-Ni alloys in their study[30]. **Figure 13** gives typical calculation results of a solidification pass and final solute profiles in primary austenite Fe-Cr-Ni alloys; the solidification path of Fe-18Cr-12Ni clearly depicts the primary austenite solidification followed by the

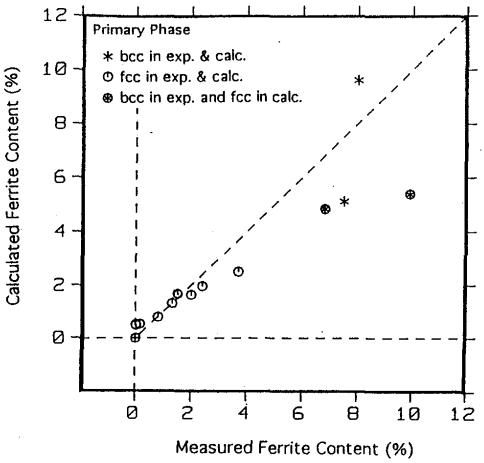

Fig. 14 Comparison of retained δ–ferrite content between calculation and mesurement [30]

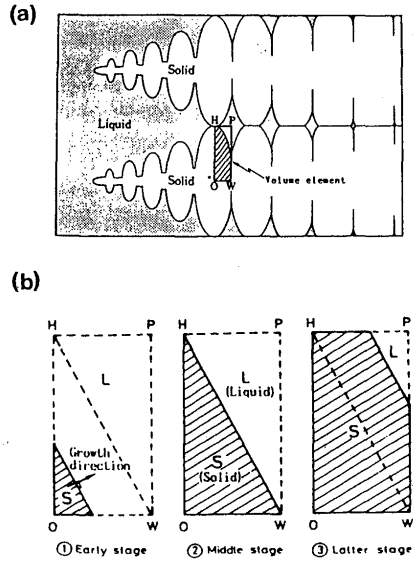

Fig. 15 (a)2–D growth of solid (b) Assumed element for FDM [32]

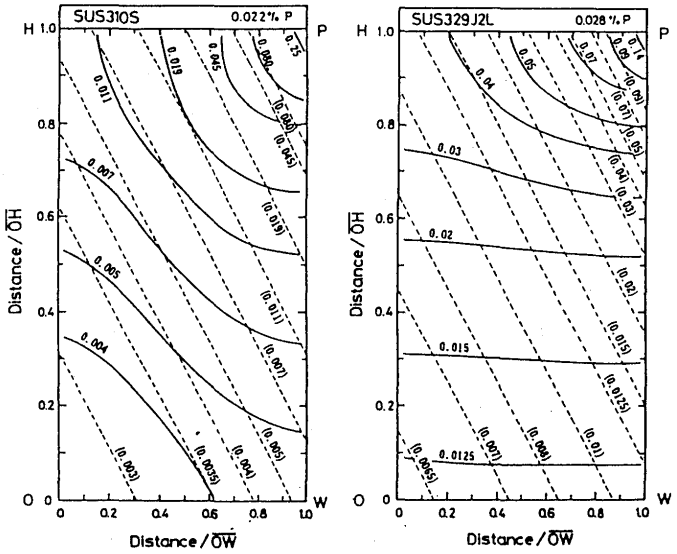

Fig. 16 Calcluated distribution of phosphorus just after the solidification in calculated area of Fig.15 [32]

eutectic solidification. This calculation enables us to estimate concentration profiles of solute atoms in a dendrite and retained δ ferrite contents of different Fe-Cr-Ni alloy weld metals. The calculation was verified to be in a good agreement with the experiments by Brooks et al.[31] as shown in **Figure 14**. In summary, the CALPHAD-assisted model was found to be effective in simulating phenomena involving multiple components and phases, provided that the thermodynamic data of the multicomponent system are assessed properly.

As to the microsegregation of solutes during a single phase solidification, Matsuda et al. [32] developed a numerical model which took account of the remaining liquid enclosed bysecondary dendrite arms. They considered a plate-like, two-dimensional dendrite as illustrated in **Figure 15**(a), and assumed the solid/liquid interface was parallel to the diagonal of a rectangular unit as in Figure 15(b) (OHPW). While solute redistribution at the solid/liquid interface was considered with the assumption of constant partition ratio, two-dimensional diffusion was calculated in the solid using FDM. **Figure 16** shows calculation results, comparing the phosphorus profiles after the solidification of the Type 310S (25Cr-20Ni) and the Type329J (22Cr-5.5Ni-3Mo-N) stainless steel weld metals. It is shown that the Type 310S weld metal retains the microsegregation of phosphorus more notably than the Type329J weld metal, and the concentration of phosphorus at the terminal stage (point P) in the former deposit is nearly twice as high as that in the latter; this is because the Type310S weld solidifies as austenite while the Type329J as ferrite, and the diffusivity of phosphorus for homogenization is much slower in the austenite than in the ferrite.

The primary application of the above model was in the final stage of the weld solidification involving the remaining liquid enclosed by secondary dendrite arms. Solidi-

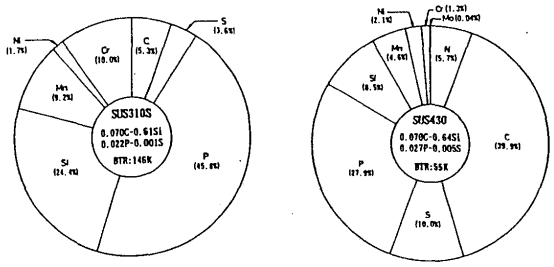

Fig. 17 Calculated effect of elements on BTR of Type 310 and Type 430 weld metal [33]

fication cracking is caused by the film-like remaining liquid and is more likely tooccur with increasing the length of the "mushy" (i.e., semisolid) zone. Thus, this model is appropriate for evaluating the solidification cracking susceptibility provided the weld metal of interest solidifies entirely as a single phase. Matsuda et al.[33] calculated the temperature range of the "mushy" zone, which is often called brittle temperature range (BTR),n using the model, and estimated the effect of each solute on the BTR. **Figure 17** shows the results for the Type3105 and Type430 (17Cr) deposits. In the Type3105 weld, phosphorus has the most adverse effect on the hot cracking susceptibility, significantly increasing the BTR, which agrees with previous investigations. In the Type430 weld, carbon is principally responsible for the BTR, although this weld metal offers low cracking susceptibility with smaller BTR than the Type3105 weld metal. These results are consistent with actual welding experiences.

The modeling of rapid solidification has increased as high energy density beams such as laser and electron beam have becomewidely used in welding, cutting, glazing, and other surface modification processes. Theconstrained growth of dendrites wastheoretically analyzed by Kurz et al. [34], andthe model has been applied to the rapidsolidification using high energy densitybeams. **Figure 18** shows an example by Nakao et al.[35] for the laser surface melting of the Type 317L stainless steel, in which theoretical Mo concentration at the dendrite tip is plotted as a function of growth velocity and compared with the actual Mo concentration measured at the dendrite cores.

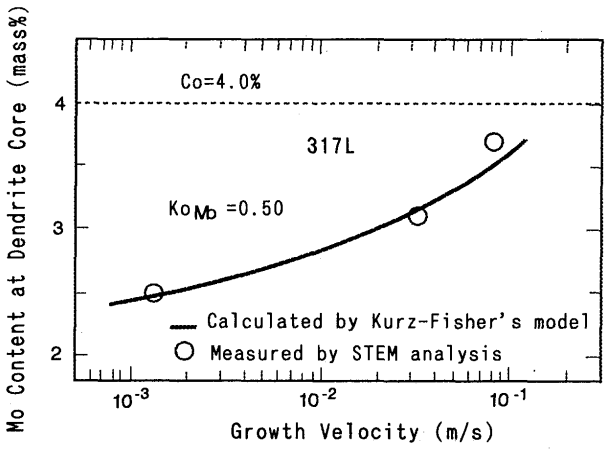

Fig. 18 Comparison between calculation and experiment on Mo concentration at the dendrite core in laser surface melted stainless steel [35]

5. Phase Transformation, Grain Growth and Segregation in Solid State

In low alloy steel weldments, the weld metal and HAZ microstructure is a function of both chemical compositions and post-solidification cooling rate. In multi-pass welding, it is also affected by the peak tem-perature and cooling rate following reheating. From the standpoint of good low temperature toughness of weldments, the enhancement of acicular ferrite formation in the as-welded condition and the decrease of martensite-austenite (M-A) constituent in an intercritically reheated zone are critical. A number of experimental studies have already been conducted on these issues. As a result, a suitable weld alloy design has been determined experimentally based on the grade of steel used, welding conditions and welding method em-ployed[9,21]. In contrast with the huge accumulation of experimental data and experiences, it appears that in Japan the amount of numerical analysis on the issues is limited. Neither the nucleation and growth kinetics of the acicular ferrite nor the thermal analysis of the formation of M-A constituent have been modeled properly.

An important factor affecting the γ-to-α transformation and hardenability of weld and HAZ is austenite grain growth during the welding thermal cycle. Grain growth during

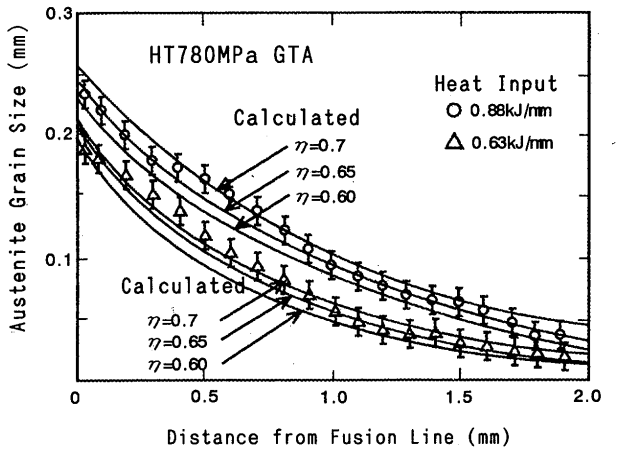

Fig. 19 Calculated austenite grain size in HAZ as a function of thermal efficiency [36]

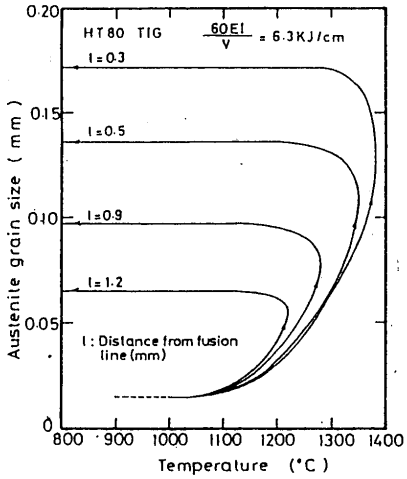

Fig. 20 Calculated austenite grain size in HAZ as a function of distance from fusion line [36]

continuous heating and cooling can be estimated by applying the additivity rule to the isothermal grain growth theory. When the thermal cycle is given by a function $q = f(t)$, then the grain size D is given by[36]:

$$D^4 - D_0^4 = K_0 \Delta t \sum_{n=0}^{i} \exp\left\{-\frac{Q}{R\left[f(t_0 + n\Delta t) + 273\right]}\right\} \quad (3)$$

where D_0 is initial grain size at time t_0, K_0 is a constant, Δt is a time increment in the additivity rule, Q is the activation energy of grain growth, and R is the universal gas constant. K_0 and Q are determined by a set of isothermal experiments. $f(t)$ can be the Rosenthal equation or any other appropriate equation for the heat conduction of welding. Ikawa et al.[36] obtained $K_0 = 2.969 \times 10^{15}$ (mm^4/s) and $Q = 5.31 \times 10^5$ (J/mol K) for the isothermal grain growth of austenite in C-Mn steels and high tensile strength steels. These values were used in the above Equation[3], and the result was compared with experiments. A result for the HAZ of a HT78OMPa steel is shown in **Figure 19**, where two arc energy levels (0.88 and 0.63 kJ/mm) of GTA welding and different thermal efficiencies, η, are examined. **Figure 20** shows the predicted grain growth behavior for different positions in the HAZ of a HT78OMPa steel GTA weld. It is noted that the austenite grain growth principally occurs on heating. Segregation to prior austenite grain boundaries is another area of concern in the welding of low alloy steels since it can cause grain boundary embrittlement and cracking during multi-pass welding and postweld heat treatment (PWHT). McLean's formula for equilibrium segregation[37] can be directly applied to the numerical modeling of a PWHT process. Ikawa et al.[38] analyzed the grain boundary segregation of phosphorus in HT-78OMPa steel welds, and verified that the prediction obtained using the McLean formula was in a good agreement with experimental observation using Auger electron spectroscopy. Yurioka et al.[39] claimed that mass transfer in equilibrium segregation should be determined on the basis of chemical potential. Using an analogy between the heat conduction equation and the activity-based diffusion equation as shown later, they derived a basic solution to the non-steady state problem of grain boundary segregation. Their solution can be simplified to the following equations under the initial condition $c(t=0)=c_0$ at the grainboundary and matrix:

at grain boundary (x=0),

$$\frac{c^{\phi}(t)}{c_0} = 1 + 2\left(\sqrt{x} - 1\right) \sum_{n=1}^{\infty} \left(\frac{\sqrt{x}-1}{\sqrt{x}+1}\right)^{n-1} erfc\left(\frac{(2n-1)w}{2\sqrt{Dt/x}}\right) \quad (4a)$$

at matrix(x>w),

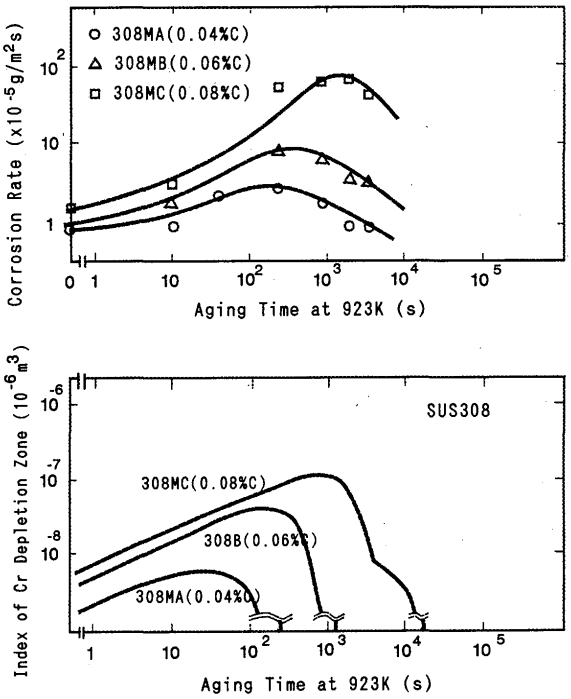

Fig. 21 Effect of aging time on Cr depletion (a) rate of intergranular corrosion (b) Cr depletion and healing [43]

$$\frac{c^M(x,t)}{c_0} = 1 - \frac{\sqrt{x}-1}{\sqrt{x}} erfc\left(\frac{x-w}{2\sqrt{Dt}}\right) + \frac{2\left(\sqrt{x}-1\right)}{\sqrt{x}\left(\sqrt{x}+1\right)} \sum_{n=1}^{\infty}\left(\frac{\sqrt{x}-1}{\sqrt{x}+1}\right)^{n-1} erfc\left(\frac{x-w+2nw\sqrt{x}}{2\sqrt{Dt}}\right) \quad (4b)$$

where c_0 is the initial concentration of the solute of interest at matrix, D is the diffusivity of the solute, w is the width of grain boundary, x is the distance from the center of grain boundary, and t is time. χ is the equilibrium segregation ratio, i.e., $\chi = c^{\phi}(t=\infty) / c^{M}(t=\infty)$, and is given by $\chi = \gamma^{M}/\gamma^{\phi}$, where γ^{ϕ} and γ^{M} are the activity coefficients of the solute at grain boundary and matrix, re-spectively. They showed that Equation (4a) is consistent with the McLean equation except at the beginning time of segregation and is a more generalized form applicable to the segregation problem in multicomponent low alloy steels. Moreover, it is possible to predict the concentration profiles of solutes in the vicinity of a grain boundary or in a depleted zone from Equation (4b).

While grain growth and grain boundary segregation are critical to low alloy steel welds subjected to multiple thermal cycles and PWHT, the precipitation of carbides and the consequent sensitization are essential issues in stainless steel welds. Applying the additivity rule to the TTP diagram of $M_{23}C_6$ carbides, Ikawa et al. [40] predicted the sensitization of the Type 304 stainless steel during weld thermal cycles. The precipitation of $M_{23}C_6$ and sigma phase and the dissolution of δ ferrite and NbC during PWHT were analyzed using the Johnson-Mehl formula[41,42]. The modeling of sensitization and its healing in austenite-ferrite duplex stainless steel welds by Nakao et al. [43] should also be acknowledged. They assumed that Cr carbide precipitation occurs at the γ/γ and γ/δ boundaries and causes Cr depletion in adjacent regions. Calculating the diffusion of Cr during heat treatment, they showed that the healing of the Cr depletion was relatively rapid for the precipitate at the γ/δ boundary while it was slow for the precipitate at the γ/γ boundary. The calculation result agrees with the experimental observation that the corrosion resistance of duplex welds recovers after relatively long sensitization heat treatment; these effects are shown in **Figure 21**.

6. HAZ Hardenability

The hardness of weldments has been predicted using a carbon equivalent and a cooling parameter such as $t_{8/5}$ or the cooling rate. The principal aim has been the prediction of the maximum HAZ hardness since it is well-correlated with cold cracking sus-ceptibility and other weld properties. The effect of cooling time and composition on the hardness was first taken into consideration in 1970's by Bekert and Holz.[44]. First in Japan, Arata et al.[45] proposed the following set of predictive equations for the HAZ hardness (H_V) of high-tensile strength steel welds:

$$H_M = 835C + 287 \quad (5a)$$

$$H_B = 500\left(C - \frac{Mn}{19} - \frac{Si}{68} - \frac{Ni}{45} + \frac{Cr}{9} + \frac{Mo}{9.9} + \frac{V}{2.1} + \frac{B}{0.48}\right) + 153 \quad (5b)$$

$$\log(\tau_M) = 5.9\left(C + \frac{Mn}{19} + \frac{Si}{14} + \frac{Ni}{37} + \frac{Cr}{19} + \frac{Mo}{9.1} - \frac{V}{49} + \frac{B}{0.31}\right) - 1.13 \qquad (5c)$$

$$\log(\tau_B) = -0.2\left(C - \frac{Mn}{4.3} - \frac{Si}{0.4} - \frac{Ni}{o.58} + \frac{Cr}{0.45} - \frac{Mo}{0.4} - \frac{V}{240} - \frac{B}{0.0024}\right) + 1.60 \qquad (5d)$$

$$H_V = b/\{ln(\tau) + a\} + 160 \qquad (5e)$$

In the above equations, H_M and H_B are the hardness of fully martensitic and non-martensitic regions, respectively. τ_M and τ_B are the corresponding critical $t_{8/5}$ for fully martensitic and non-martensitic microstructures, and τ is actual $t_{8/5}$. The constants, a and b, for the hardness prediction in Equation (5e) are determined simul-taneously by Equations (5a) through (5d). It is noted that $H_V = H_M$ when τ is equal to or smaller than τ_M. As seen in Equation (5c), τ_M is a function of carbon equivalent in the form of a linear combination of alloying elements. Therefore, this carbon equivalent is considered as an index of HAZ hardenability, which does not necessarily represent an absolute level of HAZ hardness but does indicate how the martensite formation in HAZ is facilitated. A relationship of this form between HAZ hardenability and carbon equivalent was first reported by Baslien[46] in 1970 and in more detailed experiments by Blondeau et al.[47] The significance of Arata's above approach is that critical cooling times describing the hardening behavior of materials as a function of chemical compositions were introduced to the prediction; this has been commonly employed in subse-quent hardness prediction models. Yurioka et al.[48] proposed another HAZ hardness esti-mation formula of an inverse trigonometric function based on the experiments using from ultra-low carbon steels to 9Ni steels, 9Cr steels and rail steels. **Figure 22** depicts the cha-racteristics of this predictive method. In the figure, the points M and B correspond to the hardness of fully martensitic and non-martensitic microstructures, respectively, and the two points are linked by the extrapolation using the arctangent

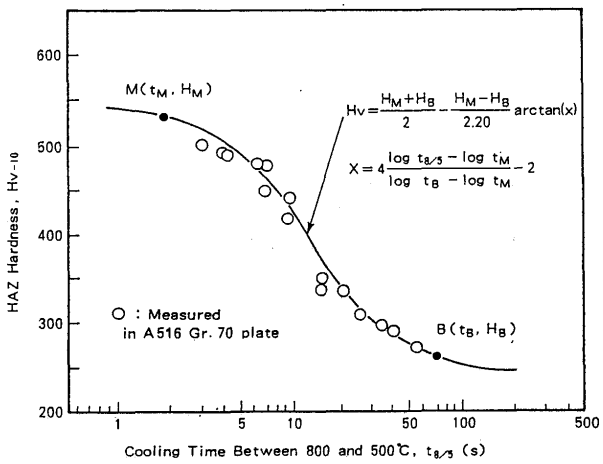

Fig. 22 Comparison between measured HAZ hardness and prediction using a formula [48]

function. This formula includes the following HAZ hardenability index like Equation (5c):

$$\tau_M = \exp(10.6CE_1 - 4.8) \qquad (6a)$$

$$CE_1 = C_P + \frac{Si}{24} + \frac{Mn}{6} + \frac{Cu}{15} + \frac{Ni}{12} + \frac{Mo}{4} + \frac{Cr\left(1 - 0.16\sqrt{Cr}\right)}{8} + \Delta H \qquad (6b)$$

where, C_P is defined as C for C<0.3wt% and $C/6+0.25$ for C>0.3wt%, and ΔH, is an additional increase in HAZ hardenability due to microalloying elements and impurities. For most modern steels or relatively clean steels, ΔH is defined as 0 for B<=1ppm., 0.03 for B=2ppm., 0.06 for B=3ppm., and 0.09 for B>=4ppm. The significant effect of boron should be noted; the amount of boron necessary to suppress intragranular ferrite formation in the grain coarsened HAZ is much smaller for than that for the fine-grained base steel.

Okumura et al.[49] examined the effect of steel cleanliness on ΔH and found that the presence of oxides and sulfides in a steel reduces ΔH due to enhanced ferrite nucleation. The reduction of ΔH should be taken into account for weld metals since oxide inclusion content is sufficiently large in most weld metals, while it is normally insignificant for the HAZ of the base metal. It is known that titanium oxides in Ti-B bearing weld metals act as effective ferrite nucleation sites. Shinada et al.[50] examined the interactive effect of oxygen, nitrogen, boron, aluminum and titanium on ΔH. They indicated

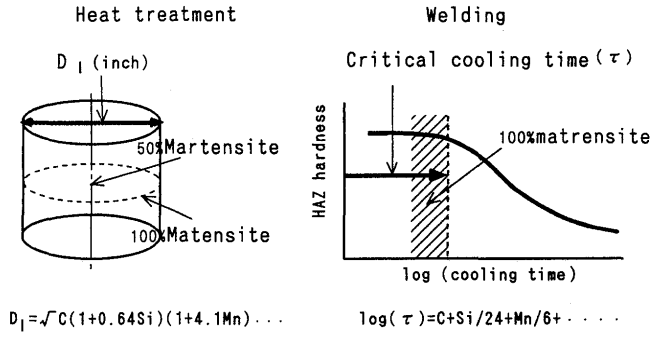

Fig. 23 Physical meaning of multiplying factor and carbon equivalent for hardenability

that Yuriokas' formula[48] also estimates the maximum hardness of a weld metal reheated by a subsequent weld pass through the evaluation of ΔH.

Terasaki et al.[51] applied the additivity rule to the Johnson-Mehl formula, and evaluated the martensite content on continuous cooling. Their predictive equation is of an expornential function type. The significance of this work is that they attempted to combine the prediction of the hardness with the transformation kinetics of steels. In other words, in their work, the predictive equation for hardness had a metallurgical basis while most of previous studies assumed hardness to be a function of cooling time.

In heat treatment of steels, hardenability of steels is described by an ideal diameter D_I, that is the critical diameter of an ideally quenched bar whose center becomes 50% martensite. The following[52] is one of the representative formulas:

$$D_1 = f(GS)\sqrt{C}(1+0.64Si)(1+4.10Mn)(1+2.83P)(1-0.62S)(1+0.27Cu)\times(1+0.52Ni)(1+2.33Cr)(1+3.14Mo)f_B \quad (7)$$

where f(GS) is a function of austenite grain size and f_B a multiplying factor for boron. The effect of boron in this formula is significant to the same extent as ΔH in Equation (6b), provided boron becomes effective. D_I is the depth of hardened zone and is expressed as a product of contents of alloying elements as seen in Equation (7). It is rational to use the hardened depth in heat treatment of steels, while it is also rational to use the cooling rate for HAZ hardenability because the cooling rate directly relates to welding conditions. This situation is shown in **Figure 23**. However, the former is of a product form of elements and the latter is of an additive form.

D_I is considered to be an alternative expression of a cooling rate because the cooling rate at the center of a quenched bar is governed by the diameter of the bar. Paying their attention to this fact, Kasuya and Yurioka[53] tried to verify the relation between the product representation in D_I and the additive representation in τ .They expanded $\tau = exp(C, Si, \ldots)$ into a Taylor series around C=0.12%, Si=0.30 %, and so on. A fairly agreement was obtained between the coefficients of alloying elements in D_I and τ . It was verified that carbon equivalent or the additive representation holds in HAZ hardnablity provided that the productive representation does in D_I and vice versa. Such an approach is essential to gain a detailed understanding of the phenomena, and also of practical use to evaluate the coefficient of a previously unassessed element. A similar approach has been attempted by Ogawa and Koseki[54] to determine the coefficient of nitrogen in the nickel equivalent used in the welding of stainless steel.

7. Hydrogen Diffusion

One of the important causes of cold cracking in a steel weld is the diffusion of hydrogen to a region of high cracking susceptibility. It is thus important to understand the phenomenon of hydrogen diffusion in a weld. A number of hydrogen diffusion analyses have been conducted in Japan both analytically or numerically. If hydrogen diffusion in a uniform medium is assumed, the driving force for diffusion (mass transfer) is the difference in mass con-centration, and then Fick's second law for mass diffusion holds. Cow and Chano[55], Fujii[56] and Suzuki[57] analytically solved a one-dimensional diffusion problem using Fick's second law. They calculated the total hydrogen content remaining in a weld, and attempted to find the safe condition for the avoidance of root cracking in a cold cracking test specimen in terms of the residual hydrogen

content.

Takahashi et al.[58] conducted a FDM analysis to estimate the hydrogen distribution in a multi-pass weld; as shown in **Figure 24**, the FDM calculation and experimental data are in close agreement. It follows that the analysis using Fick's second law can successfully solve the macroscopic diffusion in a steel weld. However, a steel weld is not considered to be a uniform medium for hydrogen diffusion, because it consists of base metal, HAZ and weld metal in which the microstructures differ significantly, and moreover, it is subjected to welding residual stress and strain. Therefore, Fick's second law is unable to solve microscopic diffusion, for example, the accumulation of hydrogen at the tip of notch or within the HAZ.

The driving force for mass diffusion in a heterogeneous medium is the difference in the chemical potential or the activity of a diffusion mass. Yurioka et al. [39] employed the following expressions for activity and activity coefficient in their diffusion analysis in 1979:

$$a = \gamma c \qquad (8a)$$

$$\gamma = \exp\left(\frac{PV^*}{RT}\right)\gamma_m \qquad (8b)$$

In these equations, a is activity, γ is activity coefficient, c is concentration, P is hydrostatic pressure or negative triaxial stress, V^* is partial molar volume, R is the universal gas constant, T is the absolute temperature and γ_m is relative activity coefficient. The relative activity coefficient, γ_m is dependent on the metallurgical structure of a diffusing medium, and is determined experimentally by measurement of the saturated concentration or solubility of hydrogen. Although the analysis carried out by Steigerwald et al.[59] in 1960 was not for a welding situation, their analytical analysis of hydrogen diffusion at the tip of a notch considered a triaxial stress field alone, i.e., γ_m =1 in Equation (8b). Yurioka and Ohshita[60] subsequently used the following equation for the analysis of hydrogen diffusion in terms of activity:

$$\frac{\partial a}{\partial t} = \frac{a}{\gamma}\frac{\partial \gamma}{\partial t} + \gamma\nabla\cdot\left(\frac{D}{\gamma}\nabla a\right) \qquad (9)$$

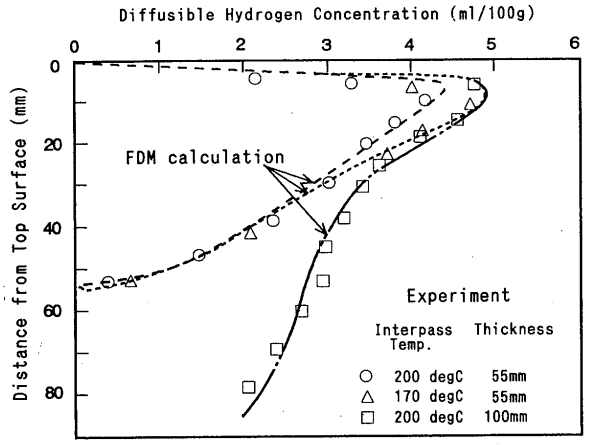

Fig. 24 FDM calculation and experiments on hydrogen distribution in a multi–pass weld [58]

where D is diffusivity of a diffusing mass. This equation is analogous to the heat conduction equation, and thus, can be evaluated using the same algorithm as employed for heat conduction. They transformed Equation (9) into a finite difference equation, and solved the hydrogen diffusion in a steel weld of heterogeneous structure under a triaxial stress field, as shown in **Figure 25**, by using FDM. One of their calculation results is shown in **Figure 26**, and indicates that the effect of preheating is significant in relation to hydrogen accumulation at the tip of a weld root notch.

Some modeling activities[61,62] similar to this approach were made using a variable ϕ like activity (chemical potential), but these neglected the law of mass conservation. In this case, Equation (9) turns into $\partial\phi/\partial t = \nabla\cdot(D\nabla\phi)$ of a Fick's second law type. It should be noted that the analytical solution described in Equation (4a) and (4b), which related to grain boundary segregation, was also derived from Equation (9), but under the condition of $\partial\gamma/\partial t$=0

8. Residual Stress

Elastic analyses of welding transient stresses started in Japan in the early 195O's. However, it was very difficult to analyze this problem using elasticity theory. To facilitate the elastic analysis, the concept of "inherent residual strain" was introduced, which made it unnecessary to calculate the transient strain

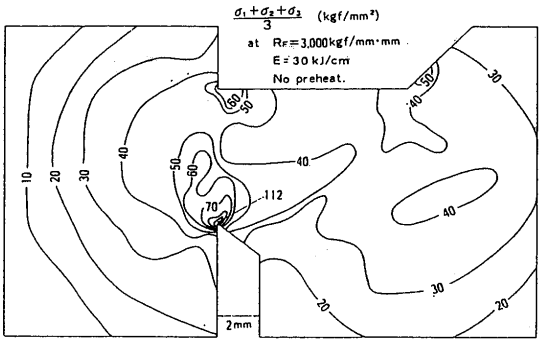

Fig. 25 FEM calculation on triaxial stress distribution in a single pass weld [60]

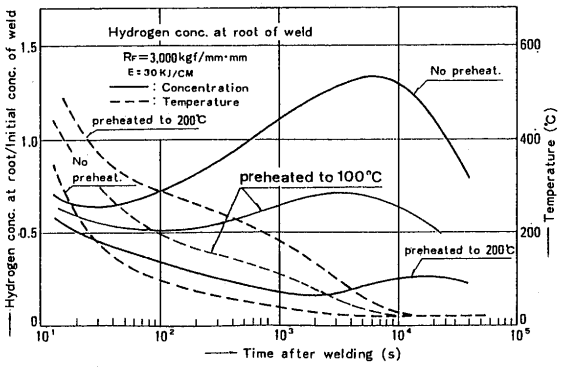

Fig. 26 Calculated hydrogen concentration at the tip of a weld notch under various preheating conditions [60]

step-by-step during post-solidification cooling[3]. The inherent residual strain is the residual plastic strain, which is a tendency toward shrinkage, remaining in a weldment after cooling to ambient temperature. Through the evaluation of the shrinkage tendency, welding residual stresses and distortion can be analyzed. The characteristic of this shrinkage tendency was represented as "inherent mismatch" by Masubuchi[3], "inherent distortion" by Watanabe and Sato[63,64] and "inherent strain" by Fujimoto[65]. This analytical method provides a solution of residual stress and distortion as an explicit function so that the parameters governing the stress and distortion can be obtained in a relatively simple way. On the other hand, this method requires characteristics of shrinkage or distortion tendency to be determined experimentally, which is termed "inherent mismatch", "inherent distortion" or "inherent strain", prior to the analysis.

In addition to the elastic analysis, there is also a thermo-elasto-plastic analysis in

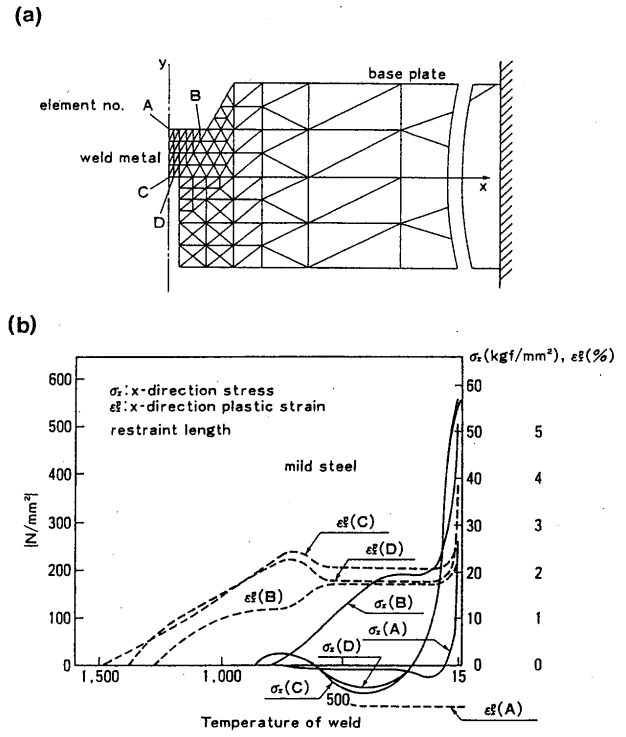

Fig. 27 FEM thermo-elasto-plastic analysis of restrained weld, (a) element system of FEM (b) transient stress and strain [70]

which transient thermal stress and strain are calculated by tracing the behavior of thermal strain step-by-step through the welding thermal cycle. This analytical research was first conducted by Watanabe[66] in Japan. Associated with advancement in computer science, numerical analysis by FEM was applied to the investigation of welding residual stress and distortion by Ueda and Yamanaka[67], Fujita and Nomoto[68], Satoh and Terasaki[69] and others. The numerical analysis enables us to determine the mechanisms and processes of initiation and growth of welding residual stress and distortion in detail. For example, the result of a FEM analysis by Ueda et al.[70], shown in **Figure 27**, depicts the.. initiation process of welding stress and strain. It is seen that an abrupt increase in welding tensile stress occurs when the joint temperature approaches ambient temperature. Yurioka and Ohshita[60] obtained the distribution of negative hydrostatic pressure or triaxial stress in a single-bevel welded joint by a FEM analysis as previously shown in Figure 25, and they extended this FEM result to a modeling of metallurgical mass transfer under a triaxial stress field. Following these early

studies, further work has been conducted to find the effects of various welding parameters including joint types (butt, fillet, and pipe-girth)[71,72], the number of welding passes[73], heat input[74] and phase transformation[75] on welding residual stresses and distortion.

9. Cold Cracking

The modeling of the HAZ cold cracking susceptibility of steel was probably started by Coe[76] who first proposed the safe welding conditions for the avoidance of cold cracking. The first studies in Japan, by Ito and Bessyo[6], proposed the following parameter for the cold cracking susceptibility of steel in 1969:

$$P_w = P_{cm} + \frac{H_D}{60} + \frac{R_F}{400,000} \qquad (10)$$

$$P_{cm} = C + \frac{Si}{30} + \frac{Mn + Cu + Cr}{20} + \frac{Ni}{60} + \frac{Mo}{15} + \frac{V}{10} + 5B \qquad (11)$$

where Pcm is the carbon equivalent, H_D is the content of diffusible hydrogen (ml /100g), and R_f is the restraint intensity of a joint (N/mm). Cold cracking can occur in many steels when a weld cools below 100℃. Some hydrogen effuses from a weld until it reaches 100℃, and it is the remaining hydrogen that promotes cold cracking. The longer the cooling time to 100℃, t_{100}, the lower the level of hydrogen remaining. It follows that cold cracking can be prevented by increasing t_{100} to a level greater than or equal to the critical cooling time, $(t_{100})_{cr}$. The cooling time t_{100} varies with welding conditions, and particularly the application of preheat will effectively extend t_{100}. Ito and Bessyo gave $(t_{100})_{cr}$ as a function of the susceptibility index, P_W;

$$(t_{100})_{cr} = 140{,}000(P_W - 0.28)^2 \qquad (12)$$

Following this initial work, a number of modeling activities for cold cracking, and the determination of safe welding conditions for the avoidance of cold cracking, have been carried out in Japan by Satoh et al.[77], Matsui and Inagaki[78], Yurioka et al.[79], Suzuki and Okumura[80] and Ito et al.[81], along with work by McParlan and Graville[82], Pavaska and Kirkaldy[83], Bragard et al.[84] and Karppi et al.[85] in other countries. However, none of these studies seems to have satisfactorily determined the safe condition for actual welding practice. This is mainly because cold cracking is a complex phenomenon; the occurrence of cold cracking is affected, either independently or interactively, by very many factors, including steel chemical composition, HAZ hardness, weld metal hydrogen content, welding heat input, welding residual stress, notch concentration factor, ambient temperature, preheating method, etc.

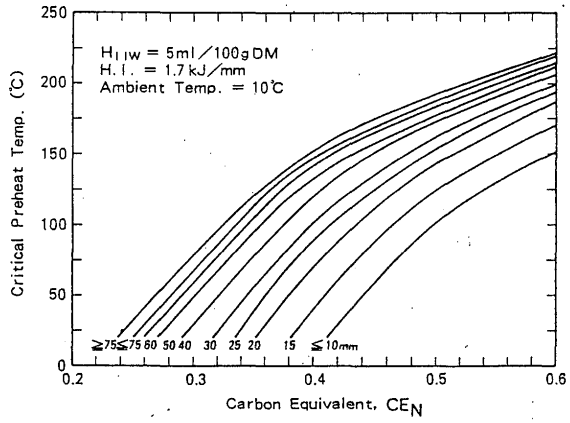

Fig. 28 Master curves for the determination of necessary preheat temperatures [86]

Yurioka[86], and Yurioka and Kasuya[87] stated that it is very difficult to model the cold cracking susceptibility of steels by such a simple mathematical expression as Equation (12); they proposed a chart method for determining the necessary preheat, in which the effect of every influential factor is included graphically. **Figure 28** shows a set of master curves in which the necessary preheat is determined by both the carbon equivalent, CE_N, and the plate or wall thickness of a steel under specific welding conditions of weld metal hydrogen, welding heat input, welding residual stress and joint restraint. The effects of these factors are also expressed in chart form, and the extent of their effects is converted into an increase or decrease in the CE_n given by

$$CE_N = C + A(C)\left\{\frac{Si}{24} + \frac{Mn}{6} + \frac{Cu}{15} + \frac{Ni}{20} + \frac{(Cr + Mo + Nb + V)}{5} + 5B\right\} \qquad (13)$$

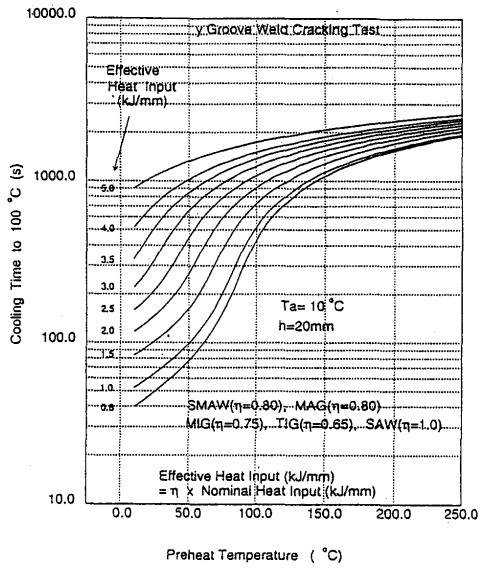

Fig. 29 A chart for cooling time to 100℃in y-groove cracking test [10]

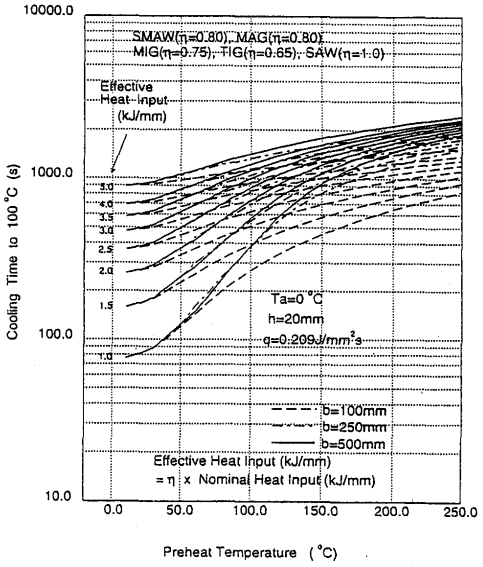

Fig. 30 A chart for cooling time to 100℃in wide plate welding [10]

where $A(C)$, is defined as $A(C) = 0.75 + 0.25 \tanh \{ 20 (C - 0.12) \}$.

In 1973, Coe[76] had already proposed a graphical method in which the IIW carbon equivalent, welding heat input, thickness and weld metal hydrogen are considered. The IIW carbon equivalent has been extensively used as an index to describe steel weldability or susceptibility to cold cracking:

$$CE_{IIW} = C + \frac{Mn}{6} + \frac{(Cu + Ni)}{15} + \frac{(Cr + Mo + V)}{5} \quad (14)$$

It is reported that the CE_{IIW} provides the best assessment of cold cracking susceptibility for carbon steels and C-Mn steels, while the *Pcm* carbon equivalent parameter in Equation (11) is most suited to carbon-reduced low alloy steels[88]. The CE_N carbon equivalent was thus proposed to assess the weldability of a wide range of steels by making CE_N approach CE_{IIW} at higher carbon levels (C>=0.16wt%) and *Pcm* in the lower carbon range (C<=0.08Wt%). The chart method uses the CE_N carbon equivalent to select welding conditions for the avoidance ofcold cracking.

Figure 28, which is based entirely on experimental results of y-groove restraint tests, gives the necessary preheat temperature for avoiding cold cracking in a small test piece. In actual welding practice, preheating is not usually conducted homogeneously as in y-groove tests, but is applied locally by gas burners or electric heaters. Therefore, the contribution of preheating to t_{100} differs between y-groove restraint testing and practical welding even when the same preheating temperature is employed. **Figure 29** shows the values of t_{100} for y-grooverestraint testing with a thickness of 20mm and an ambient temperature of 10℃, which were calculated using the Model II in the Kasuyas' heat conduction models described earlier. Also, **Figure 30** shows the values of t_{100} for the welding of wide plates locally preheated over a width of b with an ambient temperature (T_a) of 0℃, and preheating power input (q) of 0.2 J /mm^2 s, which were calculated using the linear combination of the Models I and III in the Kasuyas' models. The preheat temperature in actual welding should therefore be corrected from that for y-groove testing to the appropriate level using the chart method, so that t_{100} in practice becomes the same as that in y-groove testing. This correction step requires the graphs of t_{100} for cracking tests, such as Figure 29, and those for actual welding practice such as Figure 30.

10. Conclusion

It appears that there are two approaches to the modeling of weld phenomena. One is

seeking a simple, practical description of weldability so that feedback from the model can be readily available, even on-site, either via a PC or prepared diagrams. In this case, a simple fitting model may be sufficient as a first approximation of the weld phenomenon of interest, and can assist in a quality control of welding. The other approach to the modeling is exploring more detailed and accurate descriptions of weldability. Since weld phenomena are extremely complex, being controlled by many variables, more detailed description of the phenomena are necessary for higher precision modeling, and also for improved control of welding process and weld metallurgy. Modeling assisted by a CALPHAD (CALculation of PHAse Diagram) method is a typical example of this case. The use of thermodynamic data of multicomponent alloy systems makes it possible to describe the role of each solute, and the overall phase stability in a more realistic manner. Other examples are: a large-scale FEM analysis of residual stress, hydrogen diffusion, fluid flow in a weld pool, and so on. In the detailed approach, a number of factors are taken into consideration in a single model, and more complicated initial and boundary conditions are incorporated.

Both two approaches needs abundant experimental test data on mechanical, thermal and thermodynamic properties. The fitting model directly requires the experimental data and the theoretical modeling requires precise values for physical parameters, e.g., a CALPHAD method is based on the thermodynamic data. Accuracy of the mathematical modeling entirely relies on the precision of the experimental data. Therefore, conducting experiments for the data is important to the same extent as accomplishing mathe-matical modeling is.

References

1) S. Tanaka: J. Jpn. Weld. Soc., 13 (1943), p. 347
2) D. Rosenthal: Weld. J., 21 (1941), p. 234
3) K. Masubuchi: J. Soc. Nav. Archit. Jpn., 88 (1955), p. 189
4) Y. Ito and K. Bessyo: J. Jpn. Weld. Soc., 37(1968),p. 983
5) J. Dearden and H. O'Neil: Trns. Inst. Weld., 3 P.203(1940),
6) Y. Ito and K. Bessyo: J. Jpn. Weld. Soc., 38 (1969), P. 1134
7) T. Terasaki, T. Akiyama, K. Ishimoto, and Y. Mori: Quarterly J. Jpn. Weld. Soc., 6(1988), p. 301
8) N. Yurioka, K. Kohira and T. Yatake: J. Jpn. Weld. Soc., 43 (1974), P.921
9) T. Haze, S. Aihara, Y. Ohno, K. Uchino, Y. Kawashima, Y. Tomita, R. Chijiiwa and H. Mimura: Seitetsu-kenkyu, 326 (1987), p. 36
10) T. Kasuya and N. Yurioka: Weld. J., 72 (1993), P. 107S
11) M. Ushio and T. Ishimura: Quarterly J. Jpn. Weld. Soc., 4 (1986), p. 346
12) M. Nakatani and T. Ohji: Quarterly J. Jpn. weld. Soc., 11 (1993), p. 272
13) C. R. Heiple, J. R. Roper, R. T. Stagner, and R. J. Aden: Weld. J., 62 (1983), p. 72s
14) P. Burgardt and R. D. Campbell: Key Engr. Mater., 69&70 (1992), p. 379
15) K. C. Mills and B. J. Keene: Int'l Mater. Rev., 35 (1990), p. 185
16) G. M. Oreper, T. W. Eagar, and J. Szekely: Weld. J., 62 (1983), p. 307s
17) S. Kou and D. K. Sun: Metall. Trans. A, 16A (1985),p. 203
18) S. Yokoya, T. Okada and A. Matsunawa: Quarterly J. Jpn. Weld. Soc., 12 (1994), p. 192
19) T. Kuwana, H. Kokawa and Y. Nakata: Quarterly J. Jpn. Weld. Soc., 10(1992), p. 403
20) Y. Sato, K. Ueki, H. Kokawa and T. Kuwana: unpublished work
21) Y. Horii, S. Ohkita, M. Wakabayashi and M. Namura: Advances in Welding Science and Technology, S. A. David ed., ASM, (1986), p. 413
22) Y. Horii: Doctorial thesis to Osaka University (1995)
23) O. Grong and D. K. Matlock: Intl. Metals Reviews, 31 (1986), p. 27
24) T. Koseki and N. Yurioka: unpublished work
25) B. Sundman, B. Jansson and J.-O. Andersson: CALPHAD, 9 (198S), p. 153
26) W. Yamada, T. Matsumiya, S. Fukumoto, S. Tanaka and H. Takeuchi: Proc. of Intl Conf. on Computer-assisted Materials Design and Process Simulation, ISIJ, Tokyo, (199.3 , p. 123
27) T. W. Clyne and W. Kurz: Metall. Trans. A 12A (1981), p. 965
28) E. Scheil: Z. Metallkunde, 34 (1942), p. 70
29) H. D. Brody and M. C. Flemings: TMS-AIME, 236 (1966), p. 615
30) T. Koseki, T. Matsumiya, W. Yamada and T. Ogawa: Metall. Mater. Trans. A: 25A (1994),

p.1309
31) J. A. Brooks, J. C. williams and A. W. Thompson; Metall. Trans. 4 14A (1983) P 23
32) F. Matsuda, H. Nakagawa and J. B. Lee: Quarterly J. Jpn. Weld. Soc., 9 (1991), p. 85
33) F. Matsuda, H. Nakagawa and J. B. Lee: Quarterly J. Jpn. Weld. Soc., 9 (1991), p. 93
34) W. Kurz, B. Giovanola and R. Trivedi: Acta Metall., 34 (1986), p. 823
35) Y. Nakao, K. Nishimoto, W. P. Zhang and Y. Tamura: Quarterly J. Jpn. Weld. Soc., 9 (1991), p. 122
36) H. Ikawa, H. Oshige, S. Noi and K. Kanda: Trans. of JWS, 9, (1978), p. 41
37) D. McLean: Grain Boundaries in Metals, Oxford Press., (1957)
38) H. Ikawa, Y. Nakao and K. Nakamura: J. Jpn. Weld. Soc., 49 (1980), P. 136
39) N. Yurioka and H. Nakamura: J. Jpn. Weld. Soc., 48 (1979), p. 726
40) H. Ikawa, Y. Nakao, K. Nishimoto and N. Inoue: J. Jpn. Weld. Soc., 47 (1978 , p. 147
41) H. Ikawa, N. Arata, Y. Nakao, K. Nishimoto, T. Tanaka and S. Nakahara: J. Jpn. Weld. Soc., 46 (1977),p. 279
42) Y. Nakao, K. Nishimoto and K. Ohtani: Quarterly J. Jpn. weld. Soc., 2 (1984), p. 61
43) Y. Nakao, K. Nishimoto and M. Ishizaki: Quarterly J. Jpn. Weld. Soc., 9 (1991), p. 415
44) M. Beckert and R. Holz: Schweiss Tecknik, 23 (1973), p. 334
45) Y. Arata, K. Nishiguchi, T. Ohji and N. Kohsai: Trans. JWRI, 8 (1979), p.43
46) P. G. Bastien, J. Dollet and Ph. Maynier: MetalConstr. and British Weld. J., 49(1970), p. 9
47) R. Blondeau et al.: Heat Treatment `76, Metal Soc., London, (1976), P.I89
48) N. Yurioka, M. Okumura, T. Kasuya and H. J. U. Cotton: Metal. Constr., 19 (1987), p. 217R
49) M. Okumura, N. Yurioka and T. Kasuya: II W-I X-1459-87(1987)
50) K. Shinada, Y. Horii and N. Yurioka: Weld. J., 71 (1992), p. 253s
51) T. Terasaki, T. Nomura and T. Kitada: Quarterly J. Jpn. Weld. Soc., 6 (1988), p. 139
52) J. H. Hollomon and L. D. Jaffe: Trans. AIME, 162 (1945), p. 227
53) T. Kasuya and N. Yurioka: Weld. J., 72 (1993), p. 263s
54) T. Ogawa and T. Koseki: Weld J., 67 (1988), p.8s
55) F. R. Coe and Z. Chano: Weld. Intl., 5 (1975), p.33
56) T. Fujii: II W Doc. I X-876-74, (1974)
57) H. Suzuki: Trans. of JWS, 9 (1978), p.
58) E. Takahashi, K. Iwai and T. Horitsuji: J. Jpn. Weld. Soc., 49 (1980), p. 129
59) E. A. Steigerwald, F. W. Schaller and A. R. Troiano: TMS-AIME, 218 (1960), p. 382
60) N. Yurioka and S. Ohshita: II W Doc. I X-1161-80, (1980)
61) Y. Kikuta and S. Ochiai: II W Doc. I X-930-80, (1980)
62) V. A. Karkhin and V. G. Mikhailov: Avt. Svarka, 38 (1985), p. 39
63) M. Watanabe and K. Satoh: J. Jpn. Weld. Soc., 25(1956), p. 211
64) M. Watanabe and K. Satoh: Weld. J., 40 (1961), p. 377s
65) T. Fujimoto: J. Jpn. Weld. Soc., 39 (1970), p. 236
66) M. Watanabe: J. Jpn. Weld. Soc., 19 (1950) p.62
67) Y. Ueda and T. Yamakawa: Trans. of JWS, 2 (1971), p. 90
68) Y. Fujimoto and T. Nomoto: J. Soc. Nav. Archit. Jpn., 130 (1971), p. 183
69) K. Satoh and T. Terasaki: J. Jpn. Weld. Soc., 45 (1976), p. 42
70) Y. Ueda and Y. Kasachi: II W Doc. X-662-72, (1972)
71) K. Satoh, M. Toyoda and K. Nohara: J. Jpn. Weld. Soc., 52 (1983), p. 83
72) Y. Ueda and M. G. Yaan: Quarterly J. Jpn. Weld. Soc., 9 (1991), p. 337
73) K Satoh and T. Terasaki: J. Jpn. Weld. Soc., 45 (1976), p. 464
74) K Satoh and T. Terasaki: J. Jpn. Weld. Soc., 45 (1976), p. 150
75) K Satoh and T. Terasaki: J. Jpn. Weld. Soc., 45 (1976), p. 560
76) F. R. Coe: Welding steels without hydrogen cracking, TWI, (1973)
77) K. Satoh, T. Terasaki and Y. Okuma: J. Jpn. Weld. Soc., 48 (1974), p. 248
78) S. Matsui and M. Inagaki: II W Doc. I X-970-76, (1976)
79) N. Yurioka, H. Suzuki and S. Ohshita: Weld. J., 62 (1983), p. 147s
80) H. Suzuki and M. Okumura: Quarterly J. Jpn. weld. Soc., 2 (1984), p. 26
81) Y. Ito, M. Ikeda and M. Nakanishi: J. Jpn. Weld. Soc., 55 (1986), p. 1029
82) M. McParlan and B. A. Graville: Weld. J., 55 (1976), p. 9Ss
83) V. Pavaska and J. S. Kirkaldy: Scand. J. Metall., 11 (1982), p. 256
84) A. Bragard, J. DeFourny and M. Marquet: II W Doc. I X-1134-84, (1984)

85) R. A. Karppi, J. Runsila, M. Toyoda and K. Vartiainen: Scand. J. Metall., 13 (1984), p.66
86) N. Yurioka: The 1st US-Jpn. Symp. on Advances in Welding Metallurgy, San Fancisco, AWS, (1990), p. 51
87) N. Yurioka and T. Kasuya: Welding in the World, 35 (1995), p. 327
88) N. Yurioka and H. Suzuki: Int'l Mater. Rev., 35 (1990), p. 21